

Title: Orientation and relaxation behaviors of lamellar micro-domains of poly(methyl methacrylate)-*b*-poly(*n*-butyl acrylate) thin film as revealed by **grazing-incidence** small angle X-ray scattering.

Authors Itsuki Saito,<sup>1</sup> Daiki Shimada,<sup>1</sup> Mayu Aikawa,<sup>1</sup> Tsukasa Miyazaki,<sup>2</sup> Keisuke Shimokita,<sup>2</sup> Hideaki Takagi<sup>3</sup> and Katsuhiko Yamamoto<sup>1\*</sup>

<sup>1</sup> Department of Materials Science and Engineering, Graduate School of Engineering, Nagoya Institute of Technology, Gokiso-cho, Showa-ku, Nagoya 466-8555, Japan,

<sup>2</sup> Nitto Denko Corporation, 1-1-2, Shimohozumi, Ibaraki, Osaka 567-8680, Japan

<sup>3</sup> Photon Factory, Institute of Materials Structure Science, High Energy Accelerator Research Organization, 1-1, Oho, Tsukuba, Ibaraki 305-0801, Japan

Key words: Diblock copolymer thin film / Micro-phase separated structure / Orientation / Poly(*n*-butyl acrylate) / Grazing-incidence small angle X-ray scattering / tender X-ray

Abstract (up to 200 words)

The orientation behavior and the domain spacing relaxation of the phase-separated structure of poly(methyl methacrylate-*b*-*n*-butyl acrylate) (PMMA-*Pn*BA) thin film as investigated by **grazing-incidence small angle X-ray scattering** (GISAXS). Moreover, low-energy GISAXS (tender X-ray) was conducted for the in-depth profiling of the microphase separated structure. The PMMA-*Pn*BA forms a lamellar structure. The parallel orientation of the lamellae was induced by thermal annealing. XPS measurement indicated that the surface segregation of the *Pn*BA component occurred rapidly within one minute after annealing at 160 °C. GISAXS measurement revealed that the apparent degree of the orientation and the domain spacing  $D_{\parallel}$  of the parallel oriented lamellae increased with annealing time, the finally  $D_{\parallel}$  was close to the domain spacing of bulk. The domain spacing relaxation took longer time than the orientation of the lamellae of the BCP. Furthermore, it was found that the  $D_{\parallel}$  in the vicinity of the surface was larger than that of the inside of the film, which indicates that the domain spacing near the surface relaxed faster than the inside that is arising from the higher mobility of polymer chain.

## Introduction

Block copolymer (BCP) can form diverse structures with the periodicity of several tens nanometers both in bulk and thin film. Recently, BCP thin film has attracted great attention as an applicable material to various fields, *e.g.*, nanolithography,<sup>1-3</sup> solar cell,<sup>4-6</sup> size-selective separation,<sup>7,8</sup> adhesive material,<sup>9,10</sup> etc. In bulk state, micro-phase separated structure is predicted by the Flory-Huggins interaction parameter, the degree of polymerization and the volume fraction of blocks,<sup>11-13</sup> while in thin film, film thickness<sup>14,15</sup> and substrate-polymer interaction and/or polymer-air interaction<sup>16</sup> also must be taken into account. Although phase-separation behavior of BCP in thin film is more complicated, controlling morphology, orientation and size of the structure is necessary for practical use. This has motivated a lot of studies with respect to methodology of orientation control, such as film thickness,<sup>14,15,17,18</sup> surface free energy,<sup>18-24</sup> surface topology,<sup>19,25-27</sup> external applied-fields,<sup>28-34</sup> solvent vapor or thermal annealing,<sup>21,35-42</sup> etc.. Since functionality and physical property are also strongly related to the structure and the mobility in the vicinity of interface, describing structure in detail is required. Thus, a number of methods of characterization, such as atomic force microscopy (AFM), electron microscopy, dynamic secondary ion mass spectrometry (DSIMS), X-ray photoelectron spectroscopy (XPS), grazing-incidence small angle X-ray or neutron scattering (GISAXS, GISANS), X-ray or neutron reflectivity (XRR, NR), etc.,<sup>17,43-56</sup> have been used to study the structure of BCP thin films.

Gu *et al.* performed an in situ GISAXS measurement of a BCP thin film during solvent vapor annealing to reveal the change of micro-phase separated structure.<sup>57</sup> According to their report, the swelling ratio, *i.e.*, the thickness of swollen film divided by the original thickness, and the solvent removal rate affect not only the domain spacing but also lateral ordering. Furthermore, the swelling ratio also gives an effect on the grain size. Hence the swelling ratio and the solvent removal rate play a key role of structure development during solvent vapor annealing. Albert *et al.* investigated the effects of surface free energy on wetting behavior of BCP prepared on a Si substrate which had a nearly linear gradient in surface free energy.<sup>58</sup> They showed that the wetting behavior of poly(styrene-*b*-methyl methacrylate) on the chemically modified Si substrate strongly depends on the surface free energies. Although a lot of the researches related to the BCP morphology, orientation, wetting behaviors *etc.* has been reported,

the depth-profiling of the phase-separation behavior is still indistinct. In the phase-separation behavior of BCP thin films, the selective segregation at polymer-substrate and/or air-polymer interfaces due to the difference of surface (interfacial) free energy, orientation of microdomain, relaxation of domain spacing with different time-scale must be taken into account in order to investigate the structure development. Thus, further precise structure analysis must be conducted. In addition, higher mobility of polymer chain in the vicinity of air surface and an interaction at the interfaces cause the change of the structure and orientation along the depth.<sup>49,59,60</sup> To achieve depth-resolved structure analysis, several approaches have been employed. DSIMS can reveal BCP morphology and diffusion of polymer chain along the depth.<sup>45,46</sup> Recently, time-of-flight (ToF) SIMS with the ion cluster beam was reported to be a particularly well-suited technique that enables the in-depth profiling of polymers.<sup>61</sup> Müller-Buschbaum and co-workers have developed GISANS measurement, which possesses depth sensitivity, for BCP thin films.<sup>50,52,62</sup> Moreover, GISANS measurement provides structure information near not only air-polymer interface but also polymer-substrate surface because a neutron beam can propagate into a silicon substrate. Commonly, SAXS and GISAXS measurements have been conducted using X-ray energies of 8–13 keV (hard X-ray). However, under this condition, the X-ray penetration depth rapidly reaches micrometer order, which is generally greater than a thickness of probed films. Near the critical angle of total reflection  $\alpha_c$  at the surface, a depth-resolved GISAXS measurement with hard X-rays totally is impractical. Recently, Okuda *et al.* introduced a depth-sensitive GISAXS technique utilizing soft X-rays with an X-ray energy of 1.77 keV.<sup>63</sup> They investigated that structural relaxation near the surface and the dynamic heterogeneity of polymer chains in a thin film with this technique. We have also reported a depth-resolved structure analysis with GISAXS measurement using tender (soft) X-ray.<sup>64</sup> It was revealed that polystyrene-*b*-poly(2-vinylpyridine) thin film forming hexagonally close packed cylinder structure aligned parallel to the surface deformed along the depth direction in the thin film (thickness 420 nm), while the deformation was relaxed in the vicinity of the surface.

In this report, we investigated the phase-separation behavior of poly(methyl methacrylate-*b*-*n*-butyl acrylate) (PMMA-*Pn*BA) forming a lamellar structure aligned parallel to the substrate after appropriate thermal annealing with GISAXS measurement.

Both components of PMMA-*Pn*BA possess polarity and the phase-separated PMMA-*Pn*BA is a thermoplastic elastomer. Thus, PMMA-*Pn*BA is applicable to a pressure sensitive adhesive (PSA) material. Understanding phase-separation behavior in a film (thin film) is essentially important in order to advance the functionality as a PSA material. Herein, we inquired the structure development through such as degree of the lamellar orientation and relaxation of the lamellar domain spacing as investigated by GISAXS. The time scale of each process was also evaluated. As a result, the time scale of the orientation was shorter than that of the relaxation. Moreover, we also performed GISAXS measurement with tender X-ray for depth-resolved structure analysis. This technique revealed that the domain spacing of the lamellar structure was slightly larger in the vicinity of air surface and was close to the value of bulk state than inside of the film. This indicates that relaxation of domain spacing is faster near the air surface, arising from the higher mobility of polymer chain.

## **Experimental**

### **Materials**

Methyl methacrylate (MMA), *tert*-butyl acrylate (*t*BA) and *N,N,N',N'',N''*-pentamethyldiethylenetriamine (PMDETA) were purchased from Sigma-Aldrich Co., Ltd. *p*-Toluenesulfonyl chloride (TsCl), CuBr, anisole, 1-butanol, *p*-toluenesulfonic acid monohydrate (PTSA), toluene, *n*-hexane, methanol and tetrahydrofuran (THF) were obtained from Nacalai Tesque (Japan). MMA and *t*BA were purified by distillation over aluminum oxide granules before polymerization and other reagents were used as received.

### **Synthesis of PMMA-*b*-*Pn*BA**

To obtain PMMA-*Pn*BA ( $M_n = 32,000$ ,  $M_w/M_n = 1.17$ ,  $f_{\text{PMMA}} = 0.44$ ), poly(methyl methacrylate-*b*-*tert*-butyl acrylate) (PMMA-*Pt*BA) was synthesized via atom transfer radical polymerization (ATRP), followed by transesterification. ATRP is known as a powerful tool to synthesize various block copolymers, as comprehensively reviewed elsewhere.<sup>65</sup> Herein, a typical procedure of ATRP was used as reported previously.<sup>36,66</sup> MMA, TsCl, CuBr, OMDETA and anisole were added into a round-bottomed flask. The flask was degassed by several freeze-pump-thaw cycles, sealed in vacuum and immersed into an oil bath at 90°C for 3h to promote a polymerization reaction. After a

reaction time, the flask was exposed to air and the solution was stirred with active aluminum powders for several hours to remove the catalysts. Subsequently, PMMA macroinitiator was precipitated in large amount of *n*-hexane followed by filtration and dried in a vacuum oven. Chain extensions were performed in a similar procedure. PMMA macroinitiator, *t*BA, CuBr, PMDETA and anisole were added into a round-bottom flask. After several freeze-pump-thaw cycles, the flask was sealed and immersed into an oil bath at 100°C to start polymerization. After 24 h, the block copolymer of PMMA-*Pt*BA was precipitated in a large amount of methanol/water (9/1 vol) mixture followed by drying in a vacuum oven.

Transesterification was conducted to obtain PMMA-*Pn*BA. The synthesized PS-*Pt*BA, PTSA (0.1 equivalent of *t*BA unit), 1-butanol (10 equivalent of *t*BA unit), and toluene (to fully dissolve the block copolymer) were added into round-bottom flask. The flask was immersed into an oil bath at 120°C to conduct transesterification of *t*BA to *n*BA. After 48 h, PMMA-*Pn*BA was precipitated in a large amount of methanol followed by drying in a vacuum oven (the exchange rate > 99% revealed by NMR).

To determine molecular weight and polydispersity index of synthesized polymers, size exclusion chromatography (SEC) was carried out in the following conditions: in THF (1ml/min) at 313K on four polystyrene gel columns (Tosoh TSK) gel GMH (based size 7mm) and G400H, G200H and G100H (5mm) that were connected to a Tosoh CCPE pump (Tosoh) and ERC-7522 RI reactive index detector (ERMA Inc.). The SEC columns were calibrated against standard PMMA (Tosoh) samples.

Proton nuclear magnetic resonance (<sup>1</sup>H NMR) spectra were recorded with a Bruker 200M NMR instrument with tetramethylsilane (TMS) as the internal standard, using CDCl<sub>3</sub> as the solvent at room temperature.

### **Preparation of thin films**

For thin films, 5 wt. % polymer solutions were prepared with THF followed by spin-casting on silicon substrate at 3000 rpm for 30 seconds. Thin films were dried at room temperature. Subsequently, thermal annealing was carried out at 160°C. Thickness of the thin films was measured to be approximately 280 ± 30 nm using an optical interferometer Optical Nanogauge C10178-01 (Hamamatsu Photonics, Co., Ltd. Japan).

### **Grazing-incidence small angle X-ray scattering**

To study micro-phase separate structures in thin films, GISAXS measurement utilizing hard X-ray and tender (soft) X-ray were performed. Hard X-ray GISAXS measurement were conducted at beamlines BL6A and BL10C in Photon Factory of KEK, Tsukuba in Japan and BL03XU in SPring-8, Hyogo in Japan<sup>67,68</sup> with wavelength of 0.15 (BL6A), 0.1488 (BL10C) and 0.1 nm (BL03XU), respectively. At beamlines BL6A and BL10C, PILATUS 1M (Dectris) and PILATUS 2M (Dectris) were used as a detector which was set at a position of 2 ~ 3 m apart from sample position, respectively. In BL03XU, charge-coupled device with an image intensifier (II-CCD, Hamamatsu Photonics Co., Ltd.) was used as a detector that was set at a position of 2 m apart from sample position. Tender X-ray GISAXS measurement was performed at BL15A2 in Photon Factory. Tender and soft X-ray GISAXS recently has been used as powerful tools for surface-sensitive and depth-resolved structure analysis of thin films.<sup>63,64,69,70</sup> The BL15A2 offers X-rays in a wide energy ranging from 2.1 to 15 keV (energy resolution is  $2 \times 10^{-4}$ ). Herein, the X-ray energy was set at 2.40 keV (corresponding to the wavelength of 5.16Å) and the sample to detector distance was approximately 830 mm. To record the GISAXS image, PILATUS 2M designed for usage in vacuum was used. All detectors were calibrated with lead stearate prepared in-house ( $d = 5.01$  nm) and chicken tendon collagen ( $d = 65.3$ nm). The magnitude of the scattering vector is given by  $q = 4\pi\sin\theta/\lambda$ , where  $\lambda$  is X-ray wavelength and  $2\theta$  is the scattering angle. The scattering vector  $q_z$  denotes the component perpendicular to the film surface. The  $q_x$  and  $q_y$  are the scattering vector components in the sample surface, perpendicular to and directed to the X-ray beam, respectively. For each set  $I(y,z)$ , the detector pixels were converted into exit angle  $\alpha_f$  perpendicular to the surface and an angle  $\psi$  parallel to the surface by simple geometrical consideration resulting in a set  $I(\psi, \alpha_f)$ . Using

$$q_x = \left(\frac{2\pi}{\lambda}\right) (\cos\psi\cos\alpha_f - \cos\alpha_i), \quad (1)$$

$$q_y = \left(\frac{2\pi}{\lambda}\right) \sin\psi \sin \alpha_f, \quad (2)$$

and

$$q_z = \left(\frac{2\pi}{\lambda}\right) (\sin\alpha_i + \cos\alpha_f) \quad (3)$$

where  $\alpha_i$  is the incident angle which is defined hereafter as the angle between incident X-ray and the surface for convenience. This data set was further converted into  $I(q_y, q_z)$ .

Penetration depth of X-ray

The X-ray penetration depth  $\Lambda$  is defined as the depth where the X-ray intensity is attenuated by  $1/e$ . The value of  $\Lambda$  depends on X-ray energy (in other words, wavelength  $\lambda$ ), the critical angle,  $\alpha_c$ , of total reflection, and the angle of incidence  $\alpha_i$ . Under this definition,  $\Lambda$  is given by<sup>71</sup>

$$\Lambda = \frac{\lambda}{4\pi} \sqrt{\frac{2}{\sqrt{(\alpha_i^2 - \alpha_c^2)^2 + 4\beta^2} - (\alpha_i^2 - \alpha_c^2)}}, \quad (4)$$

where  $\beta$  is the imaginary part of the complex refractive index. The critical angle,  $\alpha_c$ ,  $\delta$  that specifies the deviation from the real part of the refractive index, and  $\beta$  are given by

$$\alpha_c = \sqrt{2\delta} \quad (5)$$

$$\delta = (r_e \lambda^2 N_A / 2\pi) \rho_M \sum_Z w_Z (f_{0Z} + f'_Z(E)) / \sum_Z w_Z A_Z \quad (6)$$

$$\beta = (r_e \lambda^2 N_A / 2\pi) \rho_M \sum_Z w_Z f''_Z(E) / \sum_Z w_Z A_Z \quad (7)$$

where  $r_e$  is the classical electron radius ( $2.82 \times 10^{-5}$  Å),  $N_A$  is Avogadro's number,  $\rho_M$  is the mass density,  $w_Z$  is the fraction of element  $Z$ ,  $A_Z$  is the relative atomic mass,  $f_{0Z}$  is the non-resonant term of the atomic scattering factor corresponding to the atomic number, and  $f'_Z(E)$  and  $f''_Z(E)$  are the real and imaginary parts of the anomalous dispersion for the incident X-ray energy  $E$ , respectively. For example, here we used  $4.2503 \times 10^{-5}$  for  $\delta$  and  $9.4521 \times 10^{-7}$  for  $\beta$  of PnBA at 2.40 keV. Furthermore, using eq 5, the critical angle of total reflection was calculated to be  $0.528^\circ$ . Figure 1 shows the calculated penetration depth of PMMA-PnBA. It is difficult to precisely control the penetration depth  $\Lambda$  at the nanometer scale for GISAXS experiment conducted using hard X-rays (1.00 or 1.50 Å) because the value of  $\Lambda$  rises abruptly at  $\alpha_c$ . However, it can be seen that as the X-ray energy decreases (wavelength increases),  $\Lambda$  changes more gradually near the critical angle and shows decreased depth values at angles greater than the critical angle. Therefore, better control of  $\Lambda$  is expected for depth-resolved GISAXS measurements using tender X-ray (2.40 keV) because of the critical angle and attenuation coefficient values that are much larger than those for the hard X-rays.

## Results and Discussion

## Orientation and relaxation of lamellar structures

2D GISAXS (hard X-ray) patterns with various annealing time were summarized in Figure 2. The 2D GISAXS pattern of as-spun sample (Figure 2a) is shaped like an ellipse which may come from **poorly ordered or kinetically frozen morphology**. Partially intense scattering was observed at  $q_z$  of  $0.25 - 0.28 \text{ nm}^{-1}$  where was emphasized due to so-called Yoneda peak, *i.e.*, it does not indicate specific orientation. This result suggests that PMMA-PnBA (as cast film) does not orient without thermal annealing. However, after thermal annealing even for 1 min, the scattering intensity at around  $q_y = 0$  *i.e.*, the sides of a beam stop, became strong. In addition, two clear ring-shaped scattering patterns similar to the Debye-Scherrer rings were observed. Each scattering can be assigned to scattering arising from transmitted X-ray (denoted as T) and reflected X-ray (denoted as R). This phenomenon is typical in the case of GISAXS measurements.<sup>72,73</sup> The scattering intensity at around  $q_y = 0$  is getting **stronger** with an increase in annealing time. This change in GISAXS patterns indicated growth of the parallel orientation of the lamellar microphase separated structure. To evaluate the degree of orientation **quantitatively, the azimuthal angle dependence of scattering intensity is normally analyzed in a case of usual transmission SAXS. In GISAXS geometry, it is quite not simple to analyze the orientation degree by this way. It may seem better way to consider the scattering intensity ratio of  $I_{parallel}$  (parallel lamellae) to  $I_{in-plane}$  (perpendicular lamellae) for estimating the degree of orientation. The scattering intensity *in-plane* at  $q_y = 0.29$  was essentially made by overlapping scatterings from transmitted and reflected X-rays and also included the Yoneda band. It is quite difficult for overlapped intensity to be deconvoluted into respective components. In addition, these scattering contributions to the *in-plane* intensity changes as the incident angle  $\alpha_c$  varies. In present experimental conditions, GISAXS patterns of thin films with different annealing times were obtained independently and each pattern was measured with different incident angles. In this situation, the change of the *in-plane* intensity depends on not only orientation but also degree of overlapping of the scatterings mentioned above. Quantitative analysis of the degree of orientation still comes with difficulty because of such reasons. Thus, in order to discuss the orientation behavior qualitatively, the apparent scattering intensity of parallel orientation ( $I_{parallel} = I_{para}^0 + I_{para,BG}$ ) was compared to the scattering intensity of random orientation ( $I_{random} = I_{ran}^0 + I_{ran,BG}$ ) as shown in Figure 3b. The value of  $I_{parallel}$  was read up from nearest position by the beam**

stop (around  $q_y$  of zero). The value of  $I_{random}$  was obtained from the position where  $q_y = 0.2 \text{ nm}^{-1}$  and  $q_z$  on the Debye-Scherrer like ring (assuming a random orientation). Both experimentally obtained intensities ( $I_{parallel}$  and  $I_{random}$ ) include essentially back ground scatterings,  $I_{para,BG}$  and  $I_{ran,BG}$ , respectively. Here, it is noted that the values of  $I_{para}^0$  (parallel component) and  $I_{ran}^0$  (random component) are veritable ones. The value of  $I_{parallel}/I_{random}$  was used as a measure of the orientation behavior although it is quite not simple to analyze quantitatively the degree of the orientation from the value of  $I_{parallel}/I_{random}$  in GISAXS because of different transmission and reflectivity of X-ray which depends on the film thickness, surface roughness, incident angles (also background) and  $I_{random}$  is still somewhat floating under the present experimental condition. Figure 3a presents the plots of the values of  $I_{parallel}/I_{random}$  as a function of annealing time. Orientation almost completed after annealing at 160 °C for 60 min.

GISAXS measurement tells a structure information about the domain spacing of the lamellar morphology. The parallel lamellar structure preferentially formed as mentioned above. The domain spacing ( $D_{||}$ ) of the lamellar structures aligned parallel to the surface was estimated. To determine the accurate domain spacing, the distorted wave Born approximation (DWBA) was applied for analysis of the GISAXS patterns. Scatterings from the transmitted X-ray (Transmission) and reflected X-ray (Reflection) are remarkable in GISAXS measurement. Peak positions of each scattering along  $q_z$  direction can be estimated using DWBA as follows<sup>72-74</sup>,

$$q_z = \frac{2\pi}{\lambda} \left[ \sin\alpha_i + \left\{ \sin^2\alpha_c + \left[ \frac{m\lambda}{D_{||}} \mp (\sin^2\alpha_i - \sin^2\alpha_c)^{1/2} \right]^2 \right\}^{1/2} \right] \quad (8)$$

where,  $m$  represents peak order, which is unity for this case. Upper (-) and lower (+) branches in the equation indicate the peak position of transmitted and reflected beam, respectively. Figure 4 shows the experimentally obtained Bragg spots as a function of the angle of incidence for PMMA-PnBA annealed for 240 min. When  $D$  was set to 21.5 nm, the calculation using eq 8 gave the best fit for all Bragg spots as shown by dashed line in Figure 4. The estimated values of the  $D_{||}$  in this way for all annealed samples were also plotted as a function of annealing time in Figure 3a. The value of the  $D_{||}$  approached to the domain spacing of the bulk sample ( $D_{bulk}$ , measured independently to be 21.6 nm) with an increase in annealing time. The domain spacing of the parallel

orientated structure was slightly smaller than that of the bulk even after thermal annealing for 4 h. The polymer chains were fixed on the substrate and the film thickness reduced during the rapid evaporation of the solvent. Consequently, the lamellar structure was deformed along the depth direction. However, thermal annealing induced the relaxation of the domain spacing. It seems taking approximately more than 2 h to complete the relaxation of  $D_{//}$  (the value of the bulk).

As is well known, preferential wetting of surface and substrate interfaces plays an important role of orientation in thin film.<sup>16,75</sup> In this case, surface energies of PMMA, PnBA and Si substrate are 41.1 mJ/m<sup>2</sup>, 33.7 mJ/m<sup>2</sup> and 77.4 ± 0.5 mJ/m<sup>2</sup>, respectively.<sup>19</sup> According to the surface free energies, it will be predicted that PMMA segregates to the surface of the silicon substrate, while PnBA segregates to air surface. As a result of preferential wetting, the parallel orientation of lamellar morphology is induced at both air and polymer/substrate interfaces and propagates into entire film.<sup>76</sup> In fact, XPS measurement revealed that molar fractions of PnBA at the surface were 80 mol% (repeat unit) as cast film and the PnBA component fully covered on the surface even after annealing with only 60 sec.

From the results as mentioned here, the segregation of each component, orientation of the lamellae, and relaxation of the domain spacing occurred in different time scale. It can be concluded that the PnBA first segregated at air surface within a minute after annealing (PMMA may segregated at the interface), second the micro-phase separated structure aligned parallel to the surface, followed by relaxation of the domain spacing. Since the intensity ratio  $I_{parallel}/I_{random}$  estimated in quite qualitative manner including large uncertainty, we will like to give a quantitative interpretation of the behaviors as much as possible in the future.

### **Structure at near surface revealed by tender X-ray GISAXS measurement**

It has been reported that the polymer thin films have different nobilities dependent on the local region, *i.e.*, near the surface, inside, or near the polymer/substrate interface. It is quite intriguing to investigate that the depth dependence of structure difference exists, in other words, whether there is difference between the structure (orientation, morphology, and *d*-spacing etc.) in the vicinity of the surface and inside of the film, or not. Okuda et.al.<sup>63</sup> and our group<sup>64</sup> have reported that tender X-ray GISAXS has a capability of depth-resolved analysis of the structure of thin films. In this study,

GISAXS measurements of PMMA-PnBA thin film thermally annealed for 2h with tender X-ray was performed with various incident angles. As shown in Figure 5a and b, in the case that  $\alpha_i$  was below  $\alpha_c$ , the scattering (marked arrows) of the lamellar structure oriented parallel to the substrate was considerably diffuse and broaden, while in the case that  $\alpha_i$  was greater than  $\alpha_c$ , the scattering became clear and sharp. The one-dimensional scattering profiles vertically cut at  $q_y$  as close to the beam stop as possible are summarized in Figure 5c. As mentioned above, the scattering peaks are assigned to be from transmission (denoted as T) and reflection (denoted as R). Peak position shifts and the magnitudes of full width at half maximum (FWHM) varied with the change of the incident angle. The shifts of the peak position can be explained with DWBA (eq 8) as shown previously in Figure 4, while the change of the FWHM can be discussed with the change of penetration depth of X-ray.<sup>63,64</sup>

The FWHM depends on the grain size of a crystal as expressed with the Laue function,  $L(q)$

$$L(\mathbf{q}_z) = \sum_N \exp(iN\mathbf{q}_z \cdot \mathbf{D}_{\parallel}) = \frac{\sin[(N+1)\mathbf{q}_z \cdot \mathbf{D}_{\parallel}/2]}{\sin[\mathbf{q}_z \cdot \mathbf{D}_{\parallel}/2]}, \quad (9)$$

where  $N$  is the number of the reflection plane. Here the attenuation decay of X-ray must be considered, *i.e.*, the X-ray wave decays exponentially. The Laue function can be re-expressed as

$$L(q_z) = \sum_N \frac{\sin[(N+1)q_z D_{\parallel}/2]}{\sin[q_z D_{\parallel}/2]} \exp\left[-\frac{ND_{\parallel}}{2\Lambda}\right] \quad (10)$$

Since the scattering intensity is proportional to the square of the Laue function, the FWHM can be calculated simply.

The FWHMs along  $q_z$  direction obtained from the scattering peak of  $D_{\parallel}$  (Transmission) were plotted as a function of incident X-ray in Figure 6. As shown in Figure 6, the FWHM remarkably decreased in the vicinity of the critical angle of total reflection. Furthermore, the calculated FWHM using eq 10 was also plotted in Figure 6. The calculated value also decreases drastically near the critical angle and indicated the identical trend with the experimental values. The experimental values are in accord with the calculated values with penetration depth  $\Lambda$  given by eq 4, indicating that the

penetration depth can be controlled in agreement with the theory. Therefore, we concluded that the depth-resolved analysis was completely performed with various incident angles in this measurement.

In the case of GISAXS measurement utilizing soft X-ray, the effect of large curvature of Ewald sphere on the GISAXS pattern cannot be negligible. Hence the curvature may affect peak position and scattering intensity (distortion scattering pattern).<sup>77</sup> If the curvature strongly affects scattering peak positions, the eq 8 must be modified. Structure analysis of the same specimen (thermally annealed for 2h) using eq 8 was performed so as to confirm whether if the eq 8 works out without any modification. Analysis of the incidence dependence of the scattering positions which were **observed** in Figure 5c using the eq 8 gave the same structural parameter,  $D_{||} = 21.4$  (inside the film) was obtained in the case of X-ray energy with 2.40 keV. Thus, it was concluded that the eq 8 worked well even in the tender X-ray regime within the observed  $q$ -range in this article.

At near the critical angle, the surface-sensitive measurement is possible as calculated with eq 4 (Figure 1). When the  $\alpha_i$  is below the  $\alpha_c$ , X-ray waves go on the film surface and cannot propagate into the film. Only the evanescent wave can penetrate from the surface into the film. In this situation, the experimentally observed scattering spot  $\alpha_s$  along the  $q_z$  direction is given by the sum of the incident angle  $\alpha_i$  and the scattering angle  $\alpha_s$  derived from the period of the observed structure. Thus,  $\alpha_s$  can be expressed as,

$$\alpha_s = \alpha_z - \alpha_i \quad (11)$$

Using eq 11, the true  $q_z$  value of the lamellar structure oriented parallel to the surface can be estimated using the experimentally observed peaks, *i.e.*  $D_{||}$  can be estimated. In the case that  $\alpha_i$  is  $0.525^\circ$  (corresponding to the  $\Lambda$  of 32.4nm),  $D_{||}$  was estimated to be 21.6 nm which is equal to the value 21.6 nm of the bulk sample. The value of  $D_{||}$  near the surface is larger than the value 21.4 nm obtained from DWBA simulation (inside the film). This indicates that relaxation of the domain spacing in the vicinity of the film surface preceded as compared to that of the inside. As reported previously, polymer chain near the surface possesses higher mobility (lower glass transition temperature or viscosity).<sup>78-80</sup> Moreover, the lamellar structure started to orient from both the air/polymer and polymer/substrate interfaces induced by segregation of one component in a BCP. Therefore, **it can be concluded that the faster relaxation of the  $d$ -spacing ( $D_{||}$ )**

of the lamellar structure near the surface resulting in reaching  $D$  of the bulk was caused by the faster segregation of P $n$ BA component at the surface and higher mobility of the polymer chains in the vicinity of the surface.

## Conclusion

We investigated the orientation behavior and the domain spacing relaxation of the phase-separated structure of poly(methyl methacrylate-*b*-*n*-butyl acrylate) (PMMA-P $n$ BA) thin film as investigated by GISAXS. The PMMA-P $n$ BA forms a lamellar structure and the lamellar structure was aligned parallel to the substrate by thermal annealing. XPS measurement indicated that the segregation of P $n$ BA (PMMA) component occurred rapidly within one minute after annealing at 160 °C. The parallel orientation of the lamellar structure was observed successfully and the domain spacing  $D_{\parallel}$  was analyzed by the DWBA calculation. GISAXS measurement revealed that the apparent degree of the orientation and the  $D_{\parallel}$  increased with annealing time, while the domain spacing relaxation took longer time than the orientation of the lamellae of the BCP. Moreover, we conducted low-energy GISAXS (tender X-ray) that enables the in-depth profiling of the microphase separated structure. It was found that the  $D_{\parallel}$  in the vicinity of the surface was larger than that of the inside of the film, which indicates that the domain spacing near the surface relaxed faster than the inside that is arising from the higher mobility of polymer chain. If the orientation behavior and precise time-dependent  $d$ -spacing are analyzed more quantitatively, the local time scale of those, which is dependent on the regions, *e.g.* near the surface and near the substrate (spatial inhomogeneity) in the film will be discussed precisely in the future work.

## Acknowledgement

This research was supported by the Ministry of Education, Culture, Sports, Science and Technology (MEXT) in Japan, Grant-in-Aid for Scientific Research (C) (26410132, 2014). GISAXS measurements were performed at the Photon Factory of High Energy Accelerator Research Organization (approval 2014G169) and at the SPring-8 (approval 2014A7214, 2014B7264, 2015A7214). Furthermore, authors thank Prof. Noriyuki Igarashi and Prof. Nobutaka Shimizu for their kind and dedicated support of low energy GISAXS at the PF.

## References

1. Singh, G., Yager, K., Berry, B., Kim, H.-C. & Karim, A. Dynamic thermal field-induced gradient soft-shear for highly oriented block copolymer thin films. *ACS Nano* **6**, 10335–10342 (2012)
2. Luo, Y., Montarnal, D., Kim, S., Shi, W., Barteau, K. P., Pester, C. W., Hustad, P. D., Christianson, M. D., Fredrickson, G. H., Kramer, E. J. & Hawker, C. J. Poly (dimethylsiloxane-*b*-methyl methacrylate): A promising candidate for Sub-10 nm patterning. *Macromolecules* **48**, 3422–3430 (2015)
3. Gu, W., Zhao, H., Wei, Q., Coughlin, E. B., Theato, P. & Russell, T. P. Line patterns from cylinder-forming photocleavable block copolymers. *Adv. Mater.* **25**, 4690–4695 (2013)
4. Zhang, Q., Cirpan, A., Russell, T. P. & Emrick, T. Donor-acceptor poly (thiophene-block-perylene diimide) copolymers: synthesis and solar cell fabrication. *Macromolecules* **42**, 1079–1082 (2009)
5. Sun, S. S., Zhang, C., Ledbetter, A., Choi, S., Seo, K., Bonner Jr, C. E., Dress, M. & Sariciftchi, N. S. Photovoltaic enhancement of organic solar cells by a bridged donor-acceptor block copolymer approach. *Appl. Phys. Lett.* **90**, 043117 (2007)
6. Crossland, E. J. W., Kamperman, M., Nedelcu, M., Ducati, C., Wiesner, U., Smilges, D.-M., Toombes, G. E. S., Hilmyer, M. A., Ludwigs, S., Steiner, U. & Snaith, H. J. A bicontinuous double gyroid hybrid solar cell. *Nano Lett.* **9**, 2807–2812 (2008)
7. Wan, L.-S., Li, J.-W., Ke, B.-B. & Xu, Z.-K. Ordered microporous membranes template by breath figures for size-selective separation. *J. Am. Chem. Soc.* **134**, 95–98 (2012)
8. Jeong, U., Ryu, D. Y., Kim, J. K., Kim, D. H., Wu, X. & Russell, T.P. Precise control of nanopore size in thin film using mixtures of asymmetric block copolymer and homopolymer. *Macromolecules* **36**, 10126–10129 (2003)
9. Brown, H. R. Effect of a diblock copolymer on the adhesion between incompatible polymers. *Macromolecules* **22**, 2859–2860 (1989)
10. Coumans, W. J., Heikens, D. & Sjoerdsma, D. Dilatometric investigation of deformation mechanisms in polystyrene-polyethylene block copolymer blends: correlation between Poisson ratio and adhesion. *Polymer* **21**, 103–108 (1980)

11. Matsen, M. W., & Bates, F. S. Unifying Weak- and Strong-Segregation Block Copolymer Theories. *Macromolecules* **29**, 1091–1098 (1996)
12. Matsen, M. W. & Schick, M. Stable and unstable phases of a diblock copolymer melt. *Phys. Rev. Lett.* **72**, 2660–2663 (1994)
13. Bates, F. S. & Fredrickson, G. H. Block copolymer thermodynamics: theory and experiment. *Annu. Rev. Phys. Chem.* **41**, 525–557 (1990)
14. Stein, G. E., Kramer, E. J., Li, X. & Wang, J. Layering transitions in thin films of spherical-domain block copolymers. *Macromolecules* **40**, 2453–2460 (2007)
15. Suh, H. S., Kang H., Nealey, P. F. & Char, K. Thickness dependence of neutral parameter windows for perpendicularly oriented block copolymer thin films. *Macromolecules* **43**, 4744–4751 (2010)
16. Albert, J. & Epps, T. H. Self-assembly of block copolymer thin films. *Materials Today* **13**, 24–44 (2010)
17. Jung, J., Park, H. W., Lee, S., Lee, H., Chang, T., Matsunaga, T. & Jinnai, H. Effect of film thickness on the phase behaviors of diblock copolymer thin film. *ACS Nano* **4**, 3109–3116 (2010)
18. Luo, M., Seppala, J. E., Albert, J. N. L., Lewis, R., Mahadevapuram, N., Stein, G. E. & Epps, T. H. Manipulating nanoscale morphologies in cylinder-forming poly(styrene-*b*-isoprene-*b*-styrene) thin films using film thickness and substrate surface chemistry gradient. *Macromolecules* **46**, 1803–1811 (2013)
19. Kim, S. O., Solak, H. H., Stoykovich, M. P., Ferrier, N. J., Pablo, J. J. & Nealey, P. F. Epitaxial self-assembly of block copolymers on lithographically defined nanopatterned substrates. *Nature* **424**, 411–414 (2003)
20. Shelton, C. K., & Epps, T. H., Decoupling substrate surface interactions in block polymer thin film self-assembly. *Macromolecules* **48**, 4572–4580 (2015)
21. Mansky, P., Liu, Y., Huang, E., Russell, T. P. & Hawker, C. Controlling polymer-surface interactions with random copolymer brushes. *Science* **275**, 1458-1460 (1997)
22. Han, E, Stuen, K. O., Leolukman, M., Liu, C.-C., Nealey, P. F. & Gopalan, P. Perpendicular orientation of domains in cylinder-forming block copolymer thick films by controlled interfacial interactions. *Macromolecules* **42**, 4896–4901 (2009)
23. Khanna, V, Cochran, E. W., Hexemer, A., Stein, G. E., Fredrickson, G. H., Kramer, E. J., Li, X., Wang, J. & Hahn, S. F. Effect of chain architecture and surface energies

- on the ordering behavior of lamellar and cylinder forming block copolymers. *Macromolecules* **39**, 9346–9356 (2006)
24. Sohn, B. H. & Yun, S. H. Perpendicular lamellae induced at the interface of neutral self-assembled monolayers in thin diblock copolymer films. *Polymer* **43**, 2507-2512 (2002)
  25. Park, S., Lee, D. H., Xu, J., Kim, B., Hong, S. W., Jeong, U., Xu, T. & Russell T. P. Macroscopic 10-terabit-per-square-inch arrays from block copolymers with lateral order. *Science* **323**, 1030–1033 (2009)
  26. Sivaniah, E., Hayashi, Y., Iino, M., Hashimoto, T. & Fukunaga, K. Observation of perpendicular orientation in symmetric diblock copolymer thin films on rough substrates. *Macromolecules* **36**, 5894-5896 (2003)
  27. Sivaniah, E., Hayashi, Y., Matsubara, S., Kiyono, S., Hashimoto, T., Fukunaga, K., Kramer, E. J. & Mates, T. Symmetric Diblock copolymer thin films on rough substrates. Kinetics and structure formation in pure block copolymer thin films. *Macromolecules* **38**, 1837–1849 (2005)
  28. Singh, G., Yager, K. G., Berry, B., Kim, H.-C. & Karim, A. Dynamic thermal field-induced gradient soft-shear for highly oriented block copolymer thin films. *ACS Nano* **6**, 10335–10342 (2012)
  29. Chremos, A., Chaikin, P. M., Register, R. A. & Panagiotopoulos, A. Sphere-to-cylinder transitions in thin films of diblock copolymers under shear: the role of wetting layers. *Macromolecules* **45**, 4406–4415 (2012)
  30. Angelescu, D. E., Waller, J. H., Adamson, D. H., Deshpande, P., Chou, S. Y., Register, R. A. & Chaikin, P. M. Macroscopic orientation of block cylinders in single-layer films by Shearing, *Adv Mater.* **16**, 1736–1740 (2004)
  31. Hong, Y.-R., Adamson, D. H., Chaikin, P. M. & Register, R. A. Shear-induced sphere-to-cylinder transition in diblock copolymer thin films. *Soft Matter* **5**, 1687–1691 (2009)
  32. Fukuhara, K., Nagano, S., Hara, M. & Seki, T. Free-surface molecular command systems for photoalignment of liquid crystalline materials. *Nat. Commun.* **5**, 3320 (2014)
  33. Sano, M., Nakamura, S., Hara, M., Nagano, S., Shinohara, Y., Amemiya, Y. & Seki, T. Pathways toward photoinduced alignment switching in liquid crystalline block copolymer films. *Macromolecules* **47**, 7178–7186 (2014)

34. Xu, T., Zvelindovsky, A. V., Sevink, G. J. A., Lyakhova, K. S., Jinnai, H. & Russell, T. P. Electric field alignment of asymmetric diblock copolymer thin films. *Macromolecules* **38**, 10788–10798 (2005)
35. Cui, G., Ohya, S., Matsutani, T., Nagano, S., Dohi, T., Nakamura, S., Sakurai, S., Miyazaki, T. & Yamamoto, K. Perpendicular orientation of sub-10 nm channels in polystyrene-*b*-poly(4-hydroxyl styrene)/PEG oligomer blend thin films. *Nanoscale* **5**, 6713–6719 (2013)
36. Cui, G., Fujikawa, M., Nagano, S., Sano, M., Takase, H., Miyazaki, T., Sakurai, S. & Yamamoto, K. Perpendicular oriented cylinders via directional coalescence of spheres embedded in block copolymer films induced by solvent annealing. *Polymer* **55**, 1601–1608 (2014)
37. Gu, W., Xu, J., Kim, J.-K., Hong, S. W., Wei, X., Yang, X., Lee, K. Y., Kuo, D. S., Xiao, S. & Russell, T. P. Solvent-assisted directed self-assembly of spherical microdomain block copolymers to high areal density arrays. *Adv. Mater.* **25**, 3677–3682 (2013).
38. Kim, S. H., Misner, M. J., Yang, L., Gang, O., Ocko, B. M. & Russell, T. P. Salt Complexation in Block Copolymer Thin Films. *Macromolecules* **39**, 8473–8479 (2006)
39. Jeong, J. W., Park, W. I., Kim, M.-J., Ross, C. A. & Jung, Y. S. Highly tunable self-assembled nanostructures from a poly(2-vinylpyridine-*b*-dimethylsiloxane) block copolymer. *Nano Lett.* **11**, 4095–4101 (2011)
40. Park, S., Wang, J.-Y., Kim, B., Xu, J. & Russell, T. P. A simple route to highly oriented and ordered nanoporous block copolymer templates. *ACS Nano* **2**, 766–772 (2008)
41. She, M.-S., Lo, T.-Y. & Ho, R.-M. Long-range ordering of block copolymer cylinders driven by combining thermal annealing and substrate functionalization. *ACS Nano* **7**, 2000–2011 (2013)
42. Edwards, E., Stoykovich, M. P., Müller, M., Solak, H. H., Pablo, J. J. & Nealey, P. F. Mechanism and kinetics of ordering in diblock copolymer thin films on chemically nanopatterned substrates. *J. Polym. Sci. B* **43**, 3444–3459 (2005)
43. van Dijk, M. A. & van den Berg, R. Ordering phenomena in thin block copolymer films studied using atomic force microscopy. *Macromolecules* **28**, 6773–6778 (1995)

44. Collin, B., Chatenay, D., Coulon, G., Ausserre, D. & Gallot, Y. Ordering of copolymer thin films as revealed by atomic force microscopy. *Macromolecules* **25**, 1621–1622 (1992)
45. Yokoyama, H., Kramer, E. J., Rafailovich, M. H., Sokolov, J. & Schwarz, S. A. Structure and diffusion of asymmetric diblock copolymers in thin films: a dynamic secondary ion mass spectrometry study. *Macromolecules* **31**, 8826–8830 (1998)
46. Coulon, G., Russell, T. P., Deline, V. R. & Green, P. F. Surface-induced orientation of symmetric, diblock copolymers: a secondary ion mass-spectrometry study. *Macromolecules* **22**, 2581–2589 (1989)
47. Zhang, J., Posselt, D., Smilgies, D.-M., Perlich, J., Kyriakos, K., Jaksch, S & Papadakis, C. M. Lamellar diblock copolymer thin films during solvent vapor annealing studied by GISAXS: Different behavior of parallel and perpendicular lamellae. *Macromolecules* **47**, 5711–5718 (2014)
48. Müller-Buschbaum, P. Grazing incidence small-angle X-ray scattering: an advanced scattering technique for the investigation of nanostructured polymer films. *Anal. Bioanal. Chem.* **376**, 3–10 (2003)
49. Choi, S., Kim, E., Ahn, H., Naidu, S., Lee, Y., Ryu, D. Y., Hawker, C. J. & Russell, T. P. Lamellar microdomain orientation and phase transition of polystyrene-*b*-poly(methyl methacrylate) films by controlled interfacial interactions. *Soft Matter* **8**, 3463–3469 (2012)
50. Müller-Buschbaum, P., Maurer, E., Bauer, E. & Cubitt, R. Surface versus confinement induced morphology transition in triblock copolymer films: a grazing incidence small angle neutron scattering investigation. *Langmuir* **22**, 9295–9303 (2006)
51. Busch, P., Posselt, D., Smilgies, D., Rauscher, M. & Papadakis, C. Inner structure of thin films of lamellar poly(styrene-*b*-butadiene) diblock copolymers as revealed by grazing-incidence small-angle scattering. *Macromolecules* **40**, 630–640 (2007)
52. Müller-Buschbaum, P., Schulz, L., Metwalli, E., Moulin, J.-F. & Cubitt, R. Lateral structures of buried interfaces in ABA-type triblock copolymer films. *Langmuir* **24**, 7639–7644 (2008).
53. Niihara, K., Matsuwaki, U., Torikai, N., Atarashi, H., Tanaka, K. & Jinnai, H. A novel structural analysis for a cylinder-forming block copolymer thin film using

- neutron reflectivity aided by transmission electron microtomography. *Macromolecules* **40**, 6940–6946 (2007)
54. Noro, A., Okuda, M., Odamaki, F., Kawaguchi, D., Torikai, N., Takano, A. & Matsushita, Y. Chain localization and interfacial thickness in microphase-separated structures of block copolymers with variable composition distributions. *Macromolecules* **39**, 7654–7661 (2006)
  55. Tokarev, I., Krenek, R., Burkov, Y., Schmeisser, D., Sidorenko, A., Minko, S. & Stamm, M. Microphase separation in thin films of poly (styrene-block-4-vinylpyridine) copolymer-2-(4'-hydroxybenzeneazo) benzoic acid assembly. *Macromolecules* **38**, 507–516 (2005)
  56. Thomas, H. R. & O'Malley, J. J. Surface studies on multicomponent polymer systems by X-ray photoelectron spectroscopy. Polystyrene/poly (ethylene oxide) diblock copolymers. *Macromolecules* **12**, 323–329 (1979)
  57. Gu, X., Gunkel, I., Hexemer, A., Gu, W. & Russell, T. P. An in situ grazing incidence X-ray scattering study of block copolymer thin films during solvent vapor annealing. *Adv. Mater.* **26**, 273–281 (2014)
  58. Albert, J. N., Baney, M. J., Stafford, C. M., Kelly, J. Y. & Epps, T. H. Generation of monolayer gradients in surface energy and surface chemistry for block copolymer thin film studies. *ACS Nano* **3**, 3977–86 (2009).
  59. Kipnusu, W. K., Elmahdy, M. M., Tress, M., Fuchs, M., Mapesa, E. U., Smilgies, D.-M., Zhang, J., Papadakis, C. M. & Kremer, F. Molecular order and dynamics of nanometric thin layers of poly (styrene-b-1, 4-isoprene) diblock copolymers. *Macromolecules* **46**, 9729–9737 (2013)
  60. Xu, T., Hawker, C. & Russell, T. P. Interfacial interaction dependence of microdomain orientation in diblock copolymer thin films. *Macromolecules* **38**, (2005)
  61. Terlier, T., Tiron, R., Gharbi, A., Chevalier, X., Veillerot, M., Martinez, E. & Barnes, J. -P. Investigation of block depth distribution in PS-b-PMMA block copolymer using ultra-low-energy cesium sputtering in TOF-SIMA. *Surf. Interface Anal.* **46**, 83–91 (2014)
  62. Busch, P., Rauscher, M., Moulin, J.-F. & Müller-Buschbaum, P. Debye–Scherrer rings from block copolymer films with powder-like order. *J. Appl. Cryst.* **44**, 370–379 (2011)

63. Okuda, H., Takeshita, K., Ochiai, S., Sakurai, S. & Kitajima, Y. Near-surface relaxation structure of annealed block copolymer film on Si substrates examined by grazing-incidence small-angle scattering utilizing soft X-rays. *J. Appl. Cryst.* **44**, 380–384 (2011)
64. Saito, I., Miyazaki, T. & Yamamoto, K. Depth-resolved structure analysis of cylindrical microdomain in block copolymer thin film by grazing-incidence small angle X-ray scattering utilizing low energy X-ray. *Macromolecules* under review
65. Matyjaszewski, K. Atom transfer radical polymerization (ATRP): current status and future perspectives. *Macromolecules* **45**, 4015–4039 (2012)
66. Cui, G., Fujikawa, M., Nagano, S., Shimokita, K., Miyazaki, T., Sakurai, S. & Yamamoto, K. Macroscopic alignment of cylinders via directional coalescence of spheres along annealing solvent permeation directions in block copolymer thick films. *Macromolecules* **47**, 5989–5999 (2014)
67. Ogawa, H., Masunaga, H., Sasaki, S., Goto, S., Tanaka, T., Seike, T., Takahashi, S., Takeshita, K., Nariyama, N., Ohashi, H., Ohata, T., Furukawa, Y., Matsushita, T., Ishizawa, Y., Yagi, N., Takata, M., Kitamura, H., Takahara, A., Sakurai, K., Tashiro, K., Kanaya, T., Amemiya, Y., Horie, K., Takenaka, M., Jinnai, H., Okuda, H., Akiba, I., Takahashi, I., Yamamoto, K., Hikosaka, M., Sakurai, S., Shinohara, Y., Sugihara, Y. & Okada, A. Experimental station for multiscale surface structural analyses of soft-material films at SPring-8 via a GISWAX/GIXD/XR-integrated system. *Polym. J.* **45**, 109-116 (2012)
68. Masunaga, H., Ogawa, H., Takano, T., Sasaki, S., Goto, S., Tanaka, T., Seike, T., Takahashi, S., Takeshita, K., Nariyama, N., Ohashi, H., Ohata, T., Furukawa, Y., Matsushita, T., Ishizawa, Y., Yagi, N., Takata, M., Kitamura, H., Sakurai, K., Tashiro, K., Takahara, A., Amamiya, Y., Horie, K., Takenaka, M., Kanaya, T., Jinnai, H., Okuda, H., Akiba, I., Takahashi, I., Yamamoto, K., Hikosaka, M., Sakurai, S., Shinohara, Y., Okada, A. & Sugihara, Y. Multipurpose soft-material SAXS&sol;WAXS&sol;GISAXS beamline at SPring-8. *Polym. J.* **43**, 471–477 (2011)
69. Ruderer, M. A., Wang, C., Schaible, E., Hexemer, A., Xu, T. & Müller-Buschbaum, P. Morphology and optical properties of P3HT:MEH-CN-PPV blend films. *Macromolecules* **46**, 4491–4501 (2013).

70. Virgili, J. M., Tao, Y., Kortright, J. B., Balsara, N. P. & Segalman, R. A. Analysis of order formation in block copolymer thin films using resonant soft X-ray scattering. *Macromolecules* **40**, 2092–2099 (2007)
71. Beiglböck, W., Ehlers, J., Hepp, K., Weidenmüller, H., Beig, R., Domcke, W., Englert, B.-G., Frisch, U., Hänggi, P., Hasinger, G., Hillebrandt, W., Jaffe, R., Janke, W., von Löhneysen, Mangano, M., Raimond, J.-M., Sornette, D., Theisen, S., Weise, W., Zittartz, J., Guinea, F., Vollhardt, D., Daillant, J. & Gibaud, A. X-ray and Neutron Reflectivity: Principles and Applications, Lect. Notes Phys. **770**. (eds Daillant, J. & Gibaud, A.) (Springer, Berlin Heidelberg, Germany, 2009)
72. Yoon, J., Yang, S. Y., Lee, B., Joo, W., Heo, K., Kim, J. K. & Ree, M. Nondestructive quantitative synchrotron grazing incidence X-ray scattering analysis of cylindrical nanostructures in supported thin films. *J. Appl. Cryst.* **40**, 305–312 (2007)
73. Busch, P., Rauscher, M., Smilgies, D.-M., Posselt, D. & Papadakis, C. M. Grazing-incidence small-angle X-ray scattering from thin polymer films with lamellar structures – the scattering cross section in the distorted-wave Born approximation. *J Appl. Cryst.* **39**, 433–442 (2006)
74. Lee, B., Park, I., Yoon, J., Park, S., Kim, J., Kim, K.-W., Chang, T. & Ree, M. Structural Analysis of Block Copolymer Thin Films with Grazing Incidence Small-Angle X-ray Scattering. *Macromolecules* **38**, 4311–4323 (2005)
75. Mansky, P., Liu, Y., Huang, E., Russell, T. P. & Hawker, C. Controlling polymer-surface interactions with random copolymer brushes. *Science* **275**, 1458–1460 (1997)
76. Russell, T. P., Coulon, G., Deline, V. R. & Miller, D. C. Characteristics of the surface-induced orientation for symmetric diblock PS/PMMA copolymers. *Macromolecules* **22**, 4600–4604 (1989)
77. Yamamoto, T., Okuda, H., Takeshita, K., Usami, N., Kitajima, Y. & Ogawa, H. Grazing-incidence small-angle X-ray scattering from Ge nanodots self-organized on Si(001) examined with soft X-rays. *J. Synchrotron Rad.* **21**, 161–164 (2014)
78. Kawaguchi, D., Tanaka, K., Kajiyama, T., Takahara, A. & Tasaki, S. Mobility gradient in surface region of monodisperse polystyrene films. *Macromolecules* **36**, 1235–1240 (2003)

79. Kajiyama, T., Tanaka, K. & Takahara, A. Depth dependence of the surface glass transition temperature of a poly (styrene-block-methyl methacrylate) diblock copolymer film on the basis of temperature-Dependent X-ray Photoelectron Spectroscopy. *Macromolecules* **28**, 3482–3484 (1995)
80. Inoue, R., Kawashima, K., Matsui, K. & Nakamura, M. Interfacial properties of polystyrene thin films as revealed by neutron reflectivity. *Phys. Rev. E* **84**, 031802 (2011)

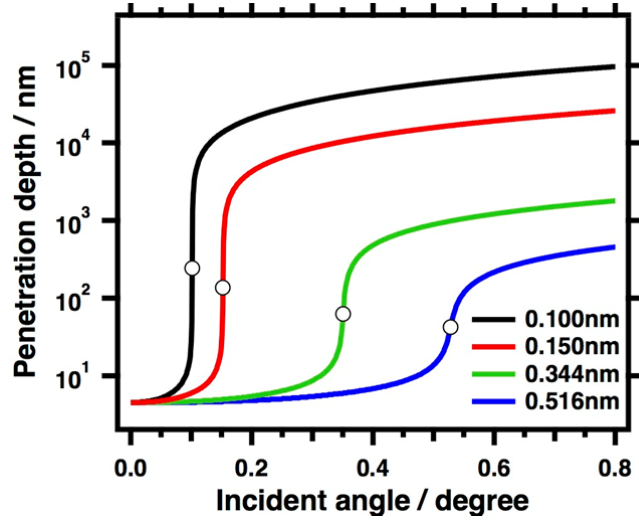


**Figure 1.** Penetration depth calculated for the present PMMA-*Pn*BA film for different X-ray wavelength (different energies). Symbol indicate the penetration depth at the critical angle of total reflection.

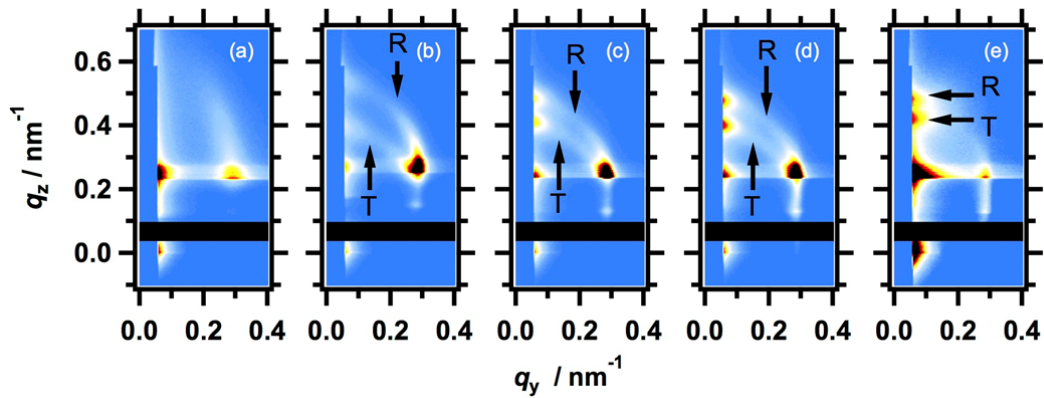


**Figure 2.** GISAXS patterns (hard X-ray, 1.488 Å) of PMMA-*Pn*BA thin as cast (a) and annealed at 160 °C with different annealing time, (b) 1, (c) 3, (d) 5, and (e) 10 min. R and T represent the scattering from reflected and transmitted X-ray beam, respectively.

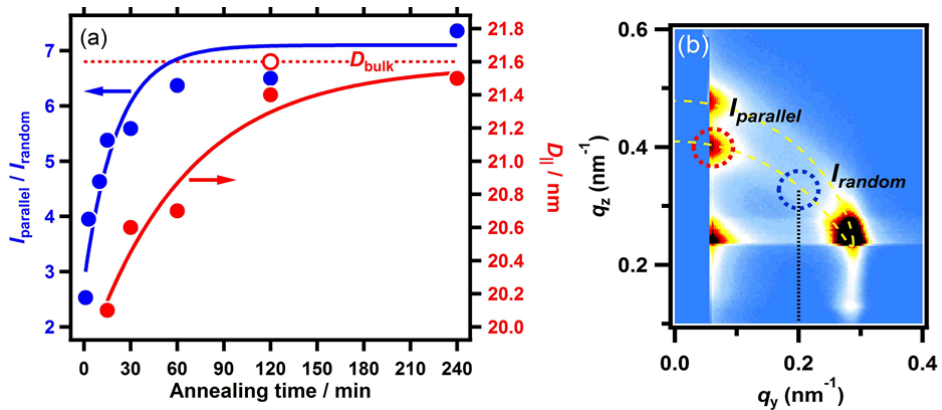
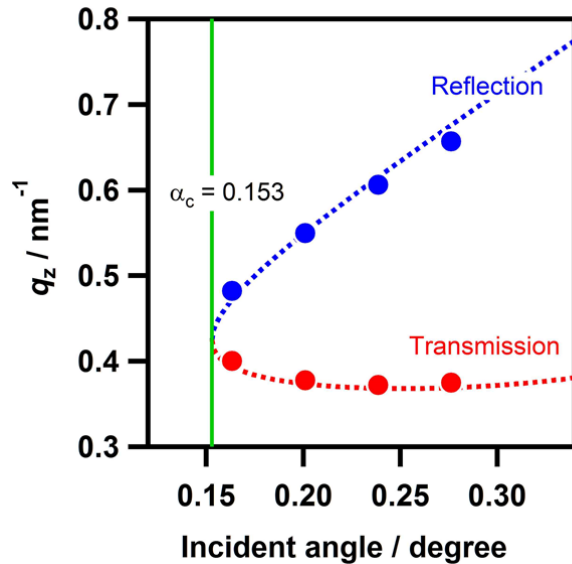
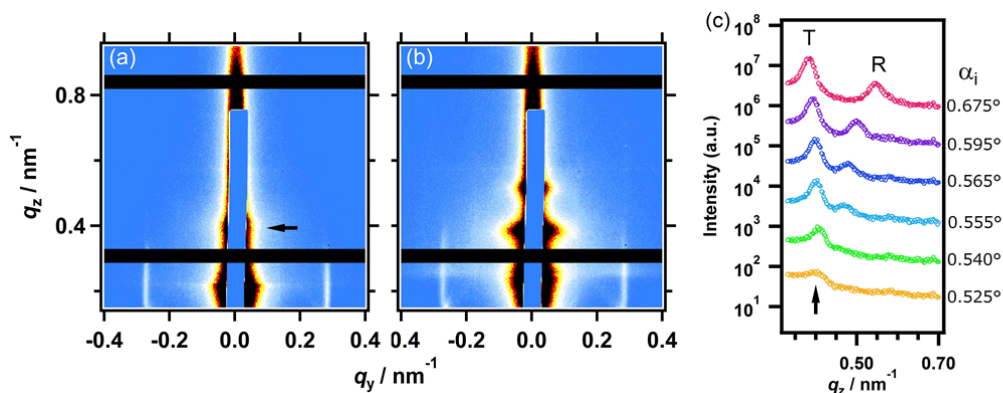


Figure 3. (a) Time evolution of

of the lamellar orientation (blue solid symbols) and the relaxation of the lamellar domain spacing (red filled symbols). The solid lines drawn as a guide to eyes. Dotted line indicates the  $D_{||}$  value of the bulk. Open circle shows the  $D_{||}$  value near the surface. The scattering intensity used for estimation of the apparent degree orientation is shown in (b). The intensity of the parallel and random components at fixed positions on the Debye-Scherrer like ring arising from transmitted X-ray (dashed curves, upper one is coming from reflected X-ray) was referred.



**Figure 4.** The incident angle dependence of the scattering positions along the  $q_z$  direction of PMMA-PnBA thin film annealed for 240 min with X-ray energy of 8.265 keV (corresponding to the wavelength of 1.5Å). Red and blue symbols represent the spots arising from transmitted and reflected X-ray, respectively. Dashed lines are the simulated  $q_z$  using eq 8 with the  $D_{||}$  of 21.5 nm and the  $\alpha_c$  of 0.153°.



**Figure 5.** Tender X-ray (2.40 keV) GISAXS patterns of PMMA-PnBA thin film annealed at 160 °C for 2 h measured at angle of incidence (a) 0.525° and (b) 0.625°. One-dimensional profiles vertically cut at  $q_y$  in the vicinity of the beam stop obtained at various incident angle  $\alpha_i$ . Each profile vertically is shifted to avoid overlapping.

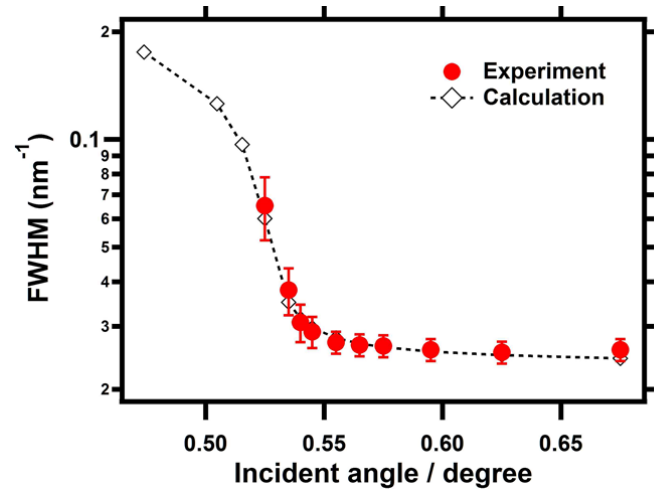


**Figure 6.** FWHM values of Bragg peak of  $D_{//}$  obtained experimentally (filled circles) and calculated (diamond and dashed line) using eq 10.